LRP 536/96 February 1996

EFFECTS OF ELECTRON-CYCLOTRON INSTABILITIES ON GYROTRON BEAM QUALITY

G. Jost, T.M. Tran, K. Appert & S. Wüthrich

Effects of electron-cyclotron instabilities on gyrotron beam quality

G. Jost, T. M. Tran, K. Appert and S. Wüthrich*

Centre de Recherches en Physique des Plasmas, Association Euratom-Confédération Suisse, Ecole Polytechnique Fédérale de Lausanne, CH-1015 Lausanne, Switzerland

* CRAY Research, PATP/PSE, EPFL, CH-1015 Lausanne, Switzerland

Abstract

A two-dimensional PIC code aimed at the investigation of electron-cyclotron beam instabilities in gyrotrons and their effects on the beam quality is presented. The code is based on recently developed techniques for handling charge conservation and open boundaries. It has been implemented on the massively parallel computer CRAY T3D. First results show an electromagnetic backward-wave instability periodically growing and decaying to energy levels close to those obtained from the electrostatic Bernstein wave instability. On the average, the resulting beam degradation is 3 to 4 times larger than that predicted by electrostatic models.

1 Introduction

The efficiency of gyrotrons depends critically on the monochromaticity in energy and velocity (or pitch angle) of the exciting electron beam [1]. Electrostatic simulations [2] of electron-cyclotron instabilities in gyrotron beam tunnels predict lower values of velocity and energy spreads than experimentally determined values which are either directly measured [3,4] or inferred from experimentally determined efficiencies [1,3,4]. Recently, parasitic frequencies have been observed in gyrotron beam tunnel [5]. It is tempting to connect the two observations and to try to explain the beam degradation with the excitation of parasitic electromagnetic modes. With this goal in mind, an electromagnetic particle-in-cell (PIC) code modeling an annular electron beam in a cylindrical cavity (beam tunnel) has been developed. The physics is assumed to be independent of the azimuthal angle which results in a two dimensional model. Only the transverse magnetic polarization is considered so far. This polarization includes, however, electrostatic perturbations of the beam and therefore allows to discuss electromagnetic instabilities together with the electrostatic ones.

In Section 2, the physical problem is presented . In Section 3, we briefly discuss the numerical scheme which is a PIC method [6,7] improved by using two recent inventions by Eastwood [8] for the current assignment and by Bérenger [9] for the treatment of boundaries open to electromagnetic waves. In Section 4 the implementation of the code on the CRAY T3D is described. Section 5 contains the results.

2 Physical problem

A cylindrical cavity (coordinates r, θ, z) of radius R_w and length L_z with a perfectly conducting wall is considered. It is immersed in an external magnetic field $\vec{B}_0 = B_0\hat{e}_z$ and is open on both ends at $z = 0$ and $z = L_z$. The electrons constituting the annular beam are injected on the left side in such a manner that their guiding centers lie on the radius R_{g0}. We restrict the model to two spatial dimensions by assuming azimuthal symmetry of both the beam and the wave fields, i.e. $\frac{\partial}{\partial\theta} = 0$. At $t = 0$, when the injection starts, there are no electrons and no electromagnetic field in the cavity. The boundary conditions at $z = 0$ and $z = L_z$ must allow the excited electromagnetic waves to leave the cavity freely without any reflections.

The beam electrons are injected into the cavity with the initial momentum defined by its axial and perpendicular components P_{z0} and $P_{\perp 0}$. Their gyrophase is chosen in such a way that the resulting beam would be as quiet as possible (in the sense of a quiet start in PIC parlance) if they were to spiral along the magnetic field $\vec{B}_0$ following unperturbed orbits. Their real orbits are then given by the relativistic equations of motion:

$$\frac{d\vec{P}}{dt} = -e(\vec{E} + \vec{v} \times \vec{B}), \tag{1}$$

$$\frac{d\vec{x}}{dt} = \vec{v}. \tag{2}$$

Here $\vec{x}$, $\vec{v}$ and $\vec{P}$ are respectively the position, the velocity and the momentum of an electron. The velocity $\vec{v}$ is related to $\vec{P}$ by $\vec{v} = \vec{P}/\gamma m$, where $\gamma = \sqrt{1 + P^2/m^2c^2}$ is the relativistic factor, m and $-e$ are the mass at rest and the charge of the electron, c is the velocity of light in vacuum; $\vec{E}$ and $\vec{B}$ are the electric and magnetic fields, respectively. Details and generalizations of the electron injection procedure will be described in a forthcoming paper.

The electromagnetic field evolves according to Maxwell's equations. For axisymmetric solutions in a cylindrical cavity they can be separated into equations describing the transverse magnetic (TM) and transverse electric (TE) polarizations. Here, we concentrate on the TM polarization which involves the field components E_r, E_z and B_θ :

$$\frac{\partial E_r}{\partial t} = -c^2\frac{\partial B_\theta}{\partial z} - \frac{1}{\epsilon_0}j_r, \tag{3}$$

$$\frac{\partial E_z}{\partial t} = c^2\frac{1}{r}\frac{\partial}{\partial r}(rB_\theta) - \frac{1}{\epsilon_0}j_z, \tag{4}$$

$$\frac{\partial B_\theta}{\partial t} = -(\frac{\partial E_r}{\partial z} - \frac{\partial E_z}{\partial r}), \tag{5}$$

where ϵ_0 is the permitivity of vacuum and $\vec{j}$ is the current density.

A subsidiary requirement for the electric field is that it satisfies the Poisson equation at all times. This can be guaranteed by imposing the charge continuity,

$$\frac{\partial \rho}{\partial t} + \vec{\nabla} \cdot \vec{j} = 0, \tag{6}$$

where ρ stands for the charge density.

3 Numerical scheme

The PIC code described in this paper is based on two non-standard features. The first is Eastwood's [8] virtual particle electromagnetic particle-mesh method for solving eqs. (1) to (5). The particularity of this method resides in the fact that eq.(6) is satisfied exactly, or in other words, that the electric field satisfies the Poisson equation at all times if it does so at $t = 0$. Algorithmically, this is achieved by using finite elements in both space and time with the result that a current due to a particle is not assigned pointwise to the mesh as in a traditional PIC method but rather "orbitwise": The current due to a particle is distributed to different mesh cells dividing it into contributions proportional to the length of its orbit in each cell. The individual contribution to a cell can be thought of as the contribution of a "virtual" particle having a charge proportional to the length of the orbit in that cell. The charge conservation obtained with this scheme is only limited by truncation errors.

The second non-standard feature of this code has to do with the open boundary conditions. It is practically impossible with a time-dependent particle-method to simulate a whole gyrotron device. In the present investigation only the beam tunnel where a uniform magnetic field favors the development of unwanted instabilities is considered. A major difficulty in the modeling of such a situation are the open electromagnetic boundaries: waves excited in the constant magnetic field region must be allowed to leave. Reflections at the boundary of the computational domain would create standing waves in contrast to reality and make the model useless. Here, we have adopted the technique of perfectly matched layers recently described by Bérenger [9] in which one uses specially devised absorbing layers of thickness L_d on both ends of the computational domain. The particularity in Bérenger's method is the use of an unphysical absorbing medium which can be matched exactly to the free space so that the theoretical reflection factor is null at any incidence angle. The field equations governing this medium are:

$$\frac{\partial E_r}{\partial t} + \frac{\sigma_E}{\epsilon_0} E_r = -c^2 \frac{\partial (B_{\theta r} + B_{\theta z})}{\partial z} - \frac{1}{\epsilon_0} j_r \tag{7}$$

$$\frac{\partial E_z}{\partial t} = c^2 \frac{1}{r} \frac{\partial}{\partial r} (r(B_{\theta r} + B_{\theta z})) - \frac{1}{\epsilon_0} j_z \tag{8}$$

$$\frac{\partial B_{\theta z}}{\partial t} + \frac{\sigma_B}{\mu_0} B_{\theta z} = -\frac{\partial E_z}{\partial r} \tag{9}$$

$$\frac{\partial B_{\theta r}}{\partial t} = \frac{\partial E_r}{\partial z} \tag{10}$$

where $B_{\theta r}$ and $B_{\theta z}$ are subcomponents of B_θ, i.e. $B_\theta = B_{\theta r} + B_{\theta z}$, σ_E and σ_B are electric and magnetic conductivities [9], respectively and μ_0 is the permeability of vacuum.

The impedance of the absorbing medium exactly matches that of the vacuum if $\sigma_E/\sigma_B = \epsilon_0/\mu_0$. In this case, the interface between the cavity and the absorbing layer does not reflect any waves back into the cavity. Reflections can occur, however, at the end of the absorbing layers at $z = -L_d$ and $z = L_z + L_d$ where $E_r = 0$ is imposed. This leads to an apparent reflection of a plane wave incident on the interface at an angle ψ if the absorption in the layer is insufficient. According to Bérenger one obtains the reflection coefficient,

$$R(\psi) = \exp\left[-\frac{2}{3}\frac{\sigma_m L_d}{\epsilon_0 c}\cos\psi\right], \tag{11}$$

for a parabolic conductivity profile of the form

$$\sigma_E(\zeta) = \sigma_m \left(\frac{\zeta}{L_d}\right)^2 \tag{12}$$

where $\zeta = -z$ in the left and $= z - L_z$ in the right absorbing layer, respectively. We usually fix σ_m such that a reflection coefficient of 0.2% results for a highly oblique incidence of 80°.

For charge conservation reasons the particles must be injected at the metallic boundary at $z = -L_d$ and traverse therefore the absorbing layers with their strange physical laws. To avoid strong wave-particle interaction in these regions we usually impede feedback by letting evolve the particles in the background magnetic field $\vec{B}_0$ alone. In this mode of operation they emit little energy in the absorbing zones. The amount can be monitored by the global non-conservation of energy because the full system, in which the particles evolve everywhere according to eq.(1), conserves the energy. The energy conservation law for the electromagnetic field written for the total volume V (cavity plus absorbing layers) is

$$\frac{\partial}{\partial t}\int_V dV\left(\frac{\epsilon_0}{2}\vec{E}^2 + \frac{1}{2\mu_0}\vec{B}^2\right) = -\int_V dV\vec{J}\cdot\vec{E} - \int_V dV\left(\frac{\sigma_B}{\mu_0^2}B_{\theta z}(B_{\theta r} + B_{\theta z}) + \sigma_E E_r^2\right), \tag{13}$$

where $\sigma_E = \sigma_B = 0$ in the cavity. Results will be shown in section 5.

The computational mesh is defined by N_z equally sized intervals along the cylinder axis and 3 equidistantly meshed zones in radial direction (fig 1). The total number of radial mesh cells is N_r. Usually, most of the cells are situated in the the beam region whose width is taken somewhat larger than two Larmor radii.

4 Implementation on parallel computer

A typical simulation of a beam tunnel of 10 cm length immersed in a static field of 3.8 Tesla is done over a time period of 14 ns. As we use an explicit time integration scheme (leap-frog) the computational timestep is limited by the CFL condition [6]. On a mesh with $N_z = 384$ and $N_r = 10 + 36 + 6 = 52$ this forces us to take 128 timesteps for one cyclotron period. A run with only 83000 particles then requires 60000 cpu-seconds on a CRAY Y-MP which is inacceptable for doing research. This is the motivation for implementing the code on a massively parallel machine like the CRAY T3D.

As the CRAY T3D has a sizable memory per processor (8 MWords) the implementation of the present code is even very simple because the total field can reside on every single processor. This allows to distribute the particles among the processors independently of their position and velocity. The field can be updated in parallel as well. For this we decompose the total cavity (i.e. cavity + absorbing regions) along the z axis into equal sub-domains $\{z_k \leq z < z_{k+1}, 0 \leq r \leq R_w\}$ and assign each one of them to a processor. Here $z_k = (k-1) \cdot N_z/N_{PE}$, k is the number of the processor, N_{PE} the total number of processors.

The following algorithm can then be used:

1. Each processor updates the positions of its resident particles and calculates their contribution to the current.
2. A parallel global sum is carried out over all the processors, computing the total current.
3. Each processor advances the field in its sub-domain.
4. Each processor sends its fields to all the other processors.
5. The total new field known, each processor updates the velocities of its particles.
6. Goto 1

This algorithm evidently provides an ideally balanced load for the processors. Its performance is, on the other hand, limited by the communication caused by the global sum and the broadcast of the subdomain fields. On a 8 processor T3D the code runs with 100000 particles at the same speed as on the Y-MP but is only four times faster with 64 processors. In this case, 45% of the time is spent for communication as shown in fig.2. This bad speed-up is due to the small particle number which is the limit of what can be run on the Y-MP. The code scales much better when more particles are used in order to decrease the numerical noise. Typically, in our computations we use 300000 particles on a 64 processor configuration. As can be seen from fig.2 in this case merely a quarter of the time is used for communication.

5 Results

The results are separated into two parts, a numerical (fig.3) and a physical one (figs.4 to 8). The performance of the numerics is, however presented in physically relevant runs and therefore we describe here the numerical together with the physical parameters. A cavity of length $L_z = 0.1\,\mathrm{m}$ and radius $R_w = 5\,\mathrm{mm}$ in a field $B_0 = 3.8\,\mathrm{T}$ has been modelled. The initial energy of the beam electrons is 80 keV and the velocity ratio, $\alpha = P_{\perp 0}/P_{z0} = 1.5$ without dispersion. The guiding center of the electrons lies at $R_{g0} = 3\,\mathrm{mm}$. The total current I of the beam is varied from 2 A to 60 A. With these parameters the beam excites the TM_{03} mode, a backward wave whose frequency and wavelength is given by the intersection between the Doppler shifted cyclotron frequency $\omega = \omega_c + k_z v_{z0}$ and the cavity dispersion relation. The cyclotron frequency is $\omega_c = eB_0/m\gamma_0 = 2\pi \times 92\,\mathrm{GHz}$ and we get for the cavity mode $\omega = 2\pi \times 85.8\,\mathrm{GHz}$ and $\lambda_z = 1.29\,\mathrm{cm}$ ($k_z = 486.2\,\mathrm{m}^{-1}$) where by λ_z and k_z we mean the wavelength and the wavenumber in axial direction.

The grid size, as already mentioned, is given by $N_z = 384$ where 2×64 intervals are used for the absorbing zones and $N_r = 52$ with 10 intervals in the center between $r = 0$ and $r = 2.5\,\mathrm{mm}$, 36 intervals between $r = 2.5\,\mathrm{mm}$ and 3.5 mm and the remaining 6 intervals between there and the wall at 5 mm. The time integration has always been performed with 128 steps per cyclotron period ($\Delta t = 8.5 \cdot 10^{-14}\,\mathrm{s}$).

With the chosen parameters, the absorbing layers have a thickness of $L_d = 2.5\,\mathrm{cm} \approx 2\lambda_z$ and a theoretical reflection coefficient, eq.(11), of 0.2% for the TM_{03} mode in question. In the present discrete version (64 intervals per absorbing zone) one measures 0.35%. This result depends on the resolution as shown by Bérenger [9]. We find 0.75% and 1.15% with a longitudinal resolution lowered by a factor 2 or 4, respectively.

The interaction between the particles and the absorbing medium can be kept small as shown in fig.3. In this figure, the electromagnetic energy emitted by the particles in the absorbing zones is plotted together with that emitted in the cavity. It is found that the ratio of these energies is at most 0.05 and this happens only at the highest currents of the order of 60 A. In the absorbing zones there is no action of the wave field on the particles. Consequently, even higher levels of emission would not influence our simulation because most of it is absorbed in the layer and only an exponentially small fraction can reach the cavity where it may influence the particles.

The charge and the energy conservation has been monitored for all the runs described in this paper. Typically, after 200000 timesteps the error in the energy was of the order of 5% of the electromagnetic energy whereas the error in the charge conservation was the round-off error [8].

Let us now turn to the physical results. The energy of the electromagnetic field in the cavity oscillates in time as will be shown in fig.5. In fig.4 we first show a snapshot of a run with $I = 2\,\mathrm{A}$ at maximum energy. The wavefield component E_z at $r = R_{g0}$ is shown as a function

of z together with the velocity dispersion measured as the standard deviation in % of P_z and $P_\perp$ of their respective average values obtained from all the particles contained in an interval $\Delta z = L_z/256$.

At a given time, we determine the maximum of the so obtained velocity spread averaged over 8 cyclotron periods and plot it against time, fig.5, together with the field energy. Also plotted in fig.5 is the electrostatic energy which has been obtained with an electrostatic PIC code [10]. The much larger energy content in the electromagnetic result is due to the unstable, backward propagating TM_{03} mode which in this 2 A case oscillates at a measured linear frequency of 86.8 GHz and exhibits an axial wavelength of 1.26 cm in good agreement with theoretical values. One remarks in fig.5 that the energy in the unstable mode periodically builds up and decays with a period of about 3.5 ns or 320 cyclotron periods. It is interesting to remark that the former period is of the order of twice the time it takes the backward propagating wave to go through the interaction area which in fig.4 has a length of about 8 cm. At higher currents the interaction length is not so neatly defined as in fig.4 but it decreases with increasing current. The dependence of the oscillation period on the current can, however, be well determined from the computations and is shown in fig.6. The period varies roughly like $1/\sqrt[3]{I}$. A similar phenomenon has been observed in the simulation of finite length electron cyclotron maser systems [11] where, however, the oscillations were rapidly damped out.

It is also interesting to remark in fig.5 that the lowest energies in the electromagnetic model coincide with the saturated values due to the Bernstein wave instability [2, 12] as observed in the electrostatic code. In the present TM model which includes the electrostatic field, the two instabilities seem to ignore each other. We have not observed the slightest correlation nor any synergy between them. This is an important result of this investigation which shows that electrostatic and electromagnetic instabilities may be treated in separate numerical models.

In order to be able to compare results from runs with different currents I the velocity dispersion is averaged over the time between the first maximum and the end of the run. In fig.6 one obtains in this way 6.5% for the spread in $P_\perp$ and 1% for that in P_z.

Before presenting the final results, we discuss in fig.7 a run where again 2 A are injected but the beam has an initial spread in velocity of 2% in both components, P_z and $P_\perp$. The reason in doing this is that spreads of this order are already obtained from time-independent calculations [13] and even higher ones are sometimes said to be produced by the surface roughness of the electron guns used in gyrotrons [14]. In the present run, the same TM_{03} backward wave mode as before is unstable but grows more slowly and saturates at a lower level than before. The resulting final velocity spread in $P_\perp$ is consequently lower than before whereas that in P_z remains close to the initial value which is higher than the final value in fig.8a. For currents higher than 10 A and a cold beam the final spread of P_z is higher than 2%. In these cases the results are not substantially modified when a hot beam is injected in place of a cold one as can be seen in fig.8.

Most remarkable in fig.8, however, is the large difference in the perpendicular velocity spread obtained with the electromagnetic model as compared to the electrostatic one. The difference

is of the order of a factor 3 to 4. In contrast to this, the spread in axial velocity is only slightly higher.

A last remark concerning fig.7 is in order. Preliminary runs over longer times have not confirmed the impression created by this figure, namely that the energy oscillations would damp out in the course of time. We have found that the behaviour in fig.7 is rather just a part of a complex nonlinear waveform whose amplitude seems not to decrease with time.

6 Conclusion

The availability at the Ecole Polytechnique Fédérale de Lausanne of a CRAY T3D has enabled us to make systematic electromagnetic PIC simulations of a gyrotron beam tunnel. The code used for these simulations has largely benefitted of the combined application of two recently invented numerical algorithms for charge conservation [8] and open boundaries [9].

The main physical result of this first investigation is the large spread in perpendicular velocity which has been obtained in fig.8a. At 2 A this spread corresponds to a spread in energy of 1%, a figure which is comparable with values inferred from experiments [4]. The experimentally measured spread in P_z [3,4] is, however, of the order of 10% for a beam current of 1.5 A and much above the values in fig.8. On the other hand, experimental observations show indeed that in quasi-optical gyrotron beam tunnels parasitic frequencies in the range of the backward wave can be excited [5]. Further experiments and numerical modelling are required to elucidate this point. In particular, the code should be completed by adding a module for the TE polarization. An additional effort should also be made to gain a clear picture of the observed low-frequency energy oscillations of the backward wave which in a gyrotron should appear as more or less transient low-frequency phenomena.

7 Acknowledgement

The authors would like to thank Dr. S. Merazzi for his help with the database MEMCOM and Dr. S. Alberti, M. Fivaz, M. Pedrozzi and Prof. M. Q. Tran for helpful discussions. This work was supported in part by the Swiss National Science Foundation, by Cray Research, Inc. within the framework of the Cray Research/EPFL Parallel Application Technology Program and by Thomson Tubes Electroniques. The computations were done on the Cray T3D massively parallel computer at EPFL, Lausanne.

8 References

1. S. Alberti et al. Physics Fluids B2 (1990)1654
2. F. S. Kuo, K. R. Chu, Chinese J. Phys. 28 (1990) 327
3. G. Soumagne,"Mesure de la fonction de distribution de vitesse du faisceau d'électrons d'un gyrotron quasi-optique", thèse N° 1390, Ecole Polytechnique de Lausanne, 1995.
4. S. Alberti, M. Pedrozzi, M.R. Siegrist, G. Soumagne, M.Q. Tran, T. M. Tran, Proc. 20th Int. Conf. on Infrared and Millimeter Waves, Orlando, December 1995.
5. M. Pedrozzi, S. Alberti, M.Q. Tran, Proc. 20th Int. Conf. on Infrared and Millimeter Waves, Orlando, December 1995.
6. C. K. Birdsall, A. B. Langdon, "Plasma Physics via Computer Simulation", Adam Hilger, New York, 1991.
7. R. W. Hockney, J. W. Eastwood, "Computer Simulation Using Particles", Institute of Physics Publishing, Bristol, 1988.
8. J. W. Eastwood, Computers Physics Communications 64 (1991) 252.
9. J-P. Bérenger, Journal of Computational Physics 114 (1994) 185.
10. T. M. Tran, G. Jost, K. Appert, O. Sauter, S. Wüthrich, Proc. 20th Int. Conf. on Infrared and Millimeter Waves, Orlando, December 1995.
11. A. T. Lin, P.K. Kaw, International Journal of Electronics 72 (1992) 887
12. V. L. Bratman, A. V. Savilov, Phys. Plasmas 2 (1995) 557
13. T. M. Tran, D. R. Whaley, S. Merazzi, R. Gruber, Proc. 6th Joint EPS-APS Int. Conf. Phys. Comput. PC94 (1994)491.
14. Sh. E. Tsimring, Radiophysics and Quantumelectronics 15(1972) 952.

9 Figures

Figure 1 : Numerical model of the cavity representing the gyrotron beam tunnel.

Figure 2 : Fraction of time spent in communication as a function of the number of particles and the number of processors on the CRAY-T3D. Shown are equilines for the fractions 0.1, 0.2, 0.3 and 0.4.

Figure 3 : Energy emitted by the particles in the absorbing zones (empty circles) and in the cavity (full circles). The energy is given as a fraction of the initial kinetic energy.

Figure 4 : Snapshot of field component E_z at $r = R_{g0}$ (a) and velocity dispersion (b) in function of z. The spread of $P_\perp$ is shown as a continuous line, that of P_z as a broken one.

Figure 5 : Electromagnetic energy (denoted W_{EM}), eletrostatic energy (denoted W_{ES}) and the maxima of the spread of $P_\perp$ and P_z as a function of time for a current equal to 2 A for the cold beam case.

Figure 6 : Oscillation period of electromagnetic energy in TM_{03} backward mode versus beam current.

Figure 7 : Electromagnetic energy (denoted W_{EM}), the maxima of the spread of $P_\perp$ and P_z as a function of time for a current equal to 2 A for the hot beam case.

Figure 8 : Maxima of the spread of $P_\perp$ (a) and the spread of P_z (b) from the electromagnetic (EM) and electrostatic (ES) computations as a function of current. The initial velocity dispersion of the beam is indicated by the words "hot" and "cold".

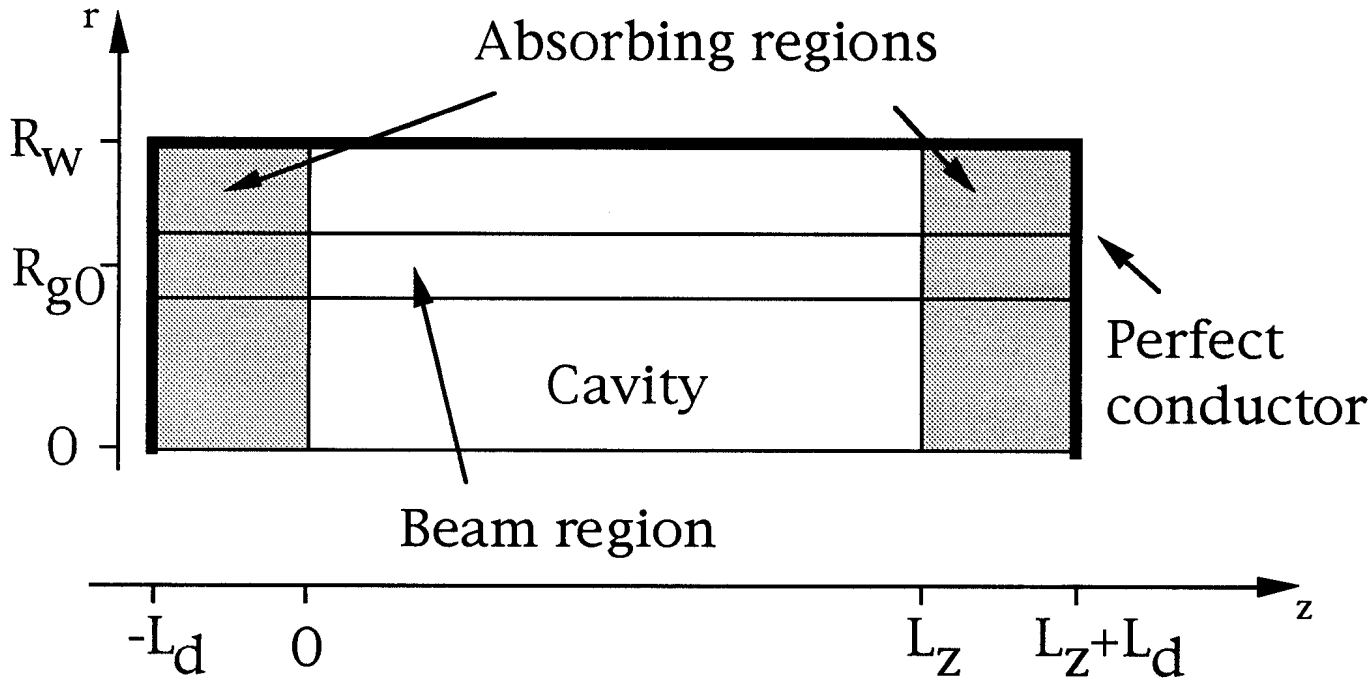
r
Absorbing regions
R_W
R_{g0}
0
Cavity
Perfect
conductor
Beam region
z
$-L_d$
0
L_z
L_z+L_d

Figure 1

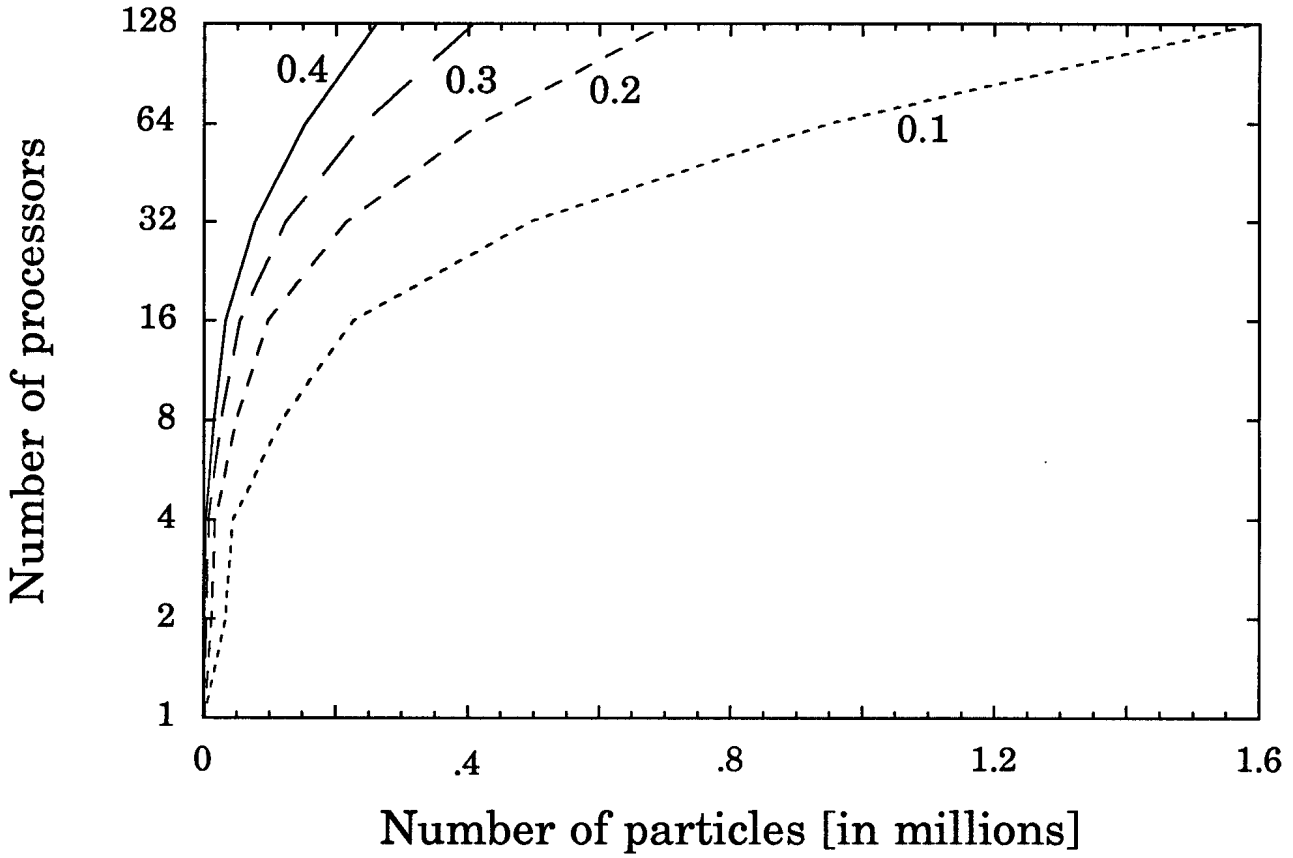

Figure 2

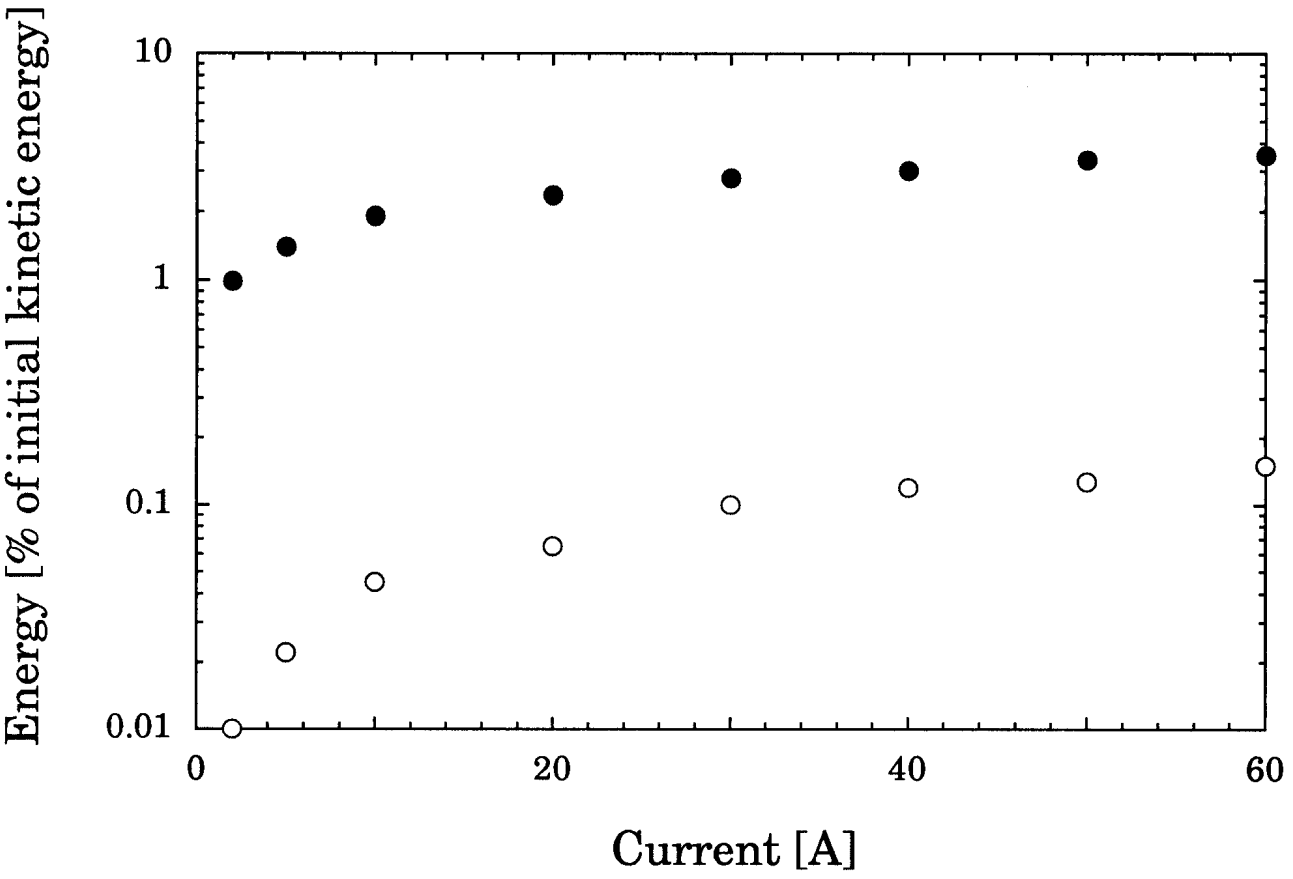

Figure 3

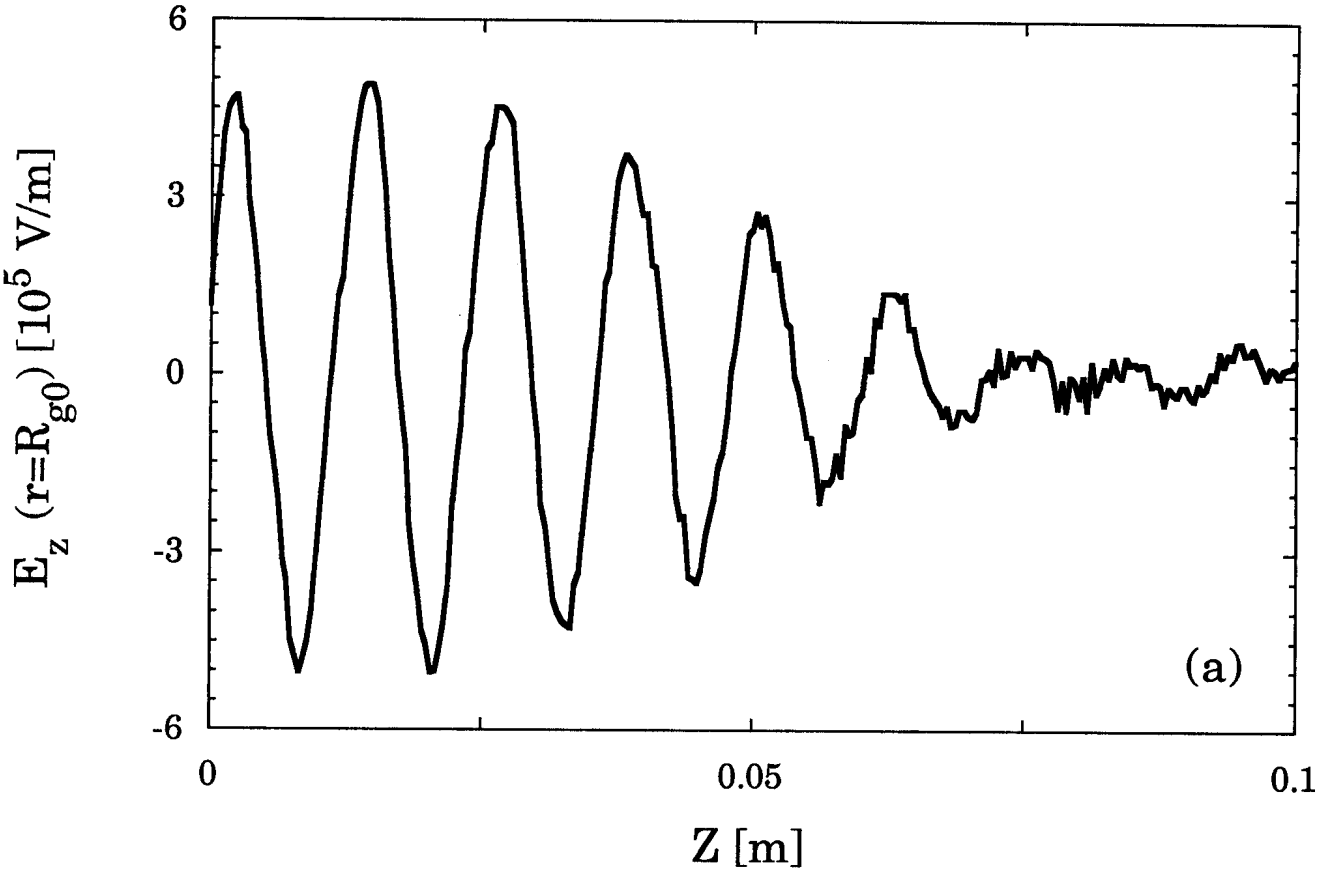

Figure 4

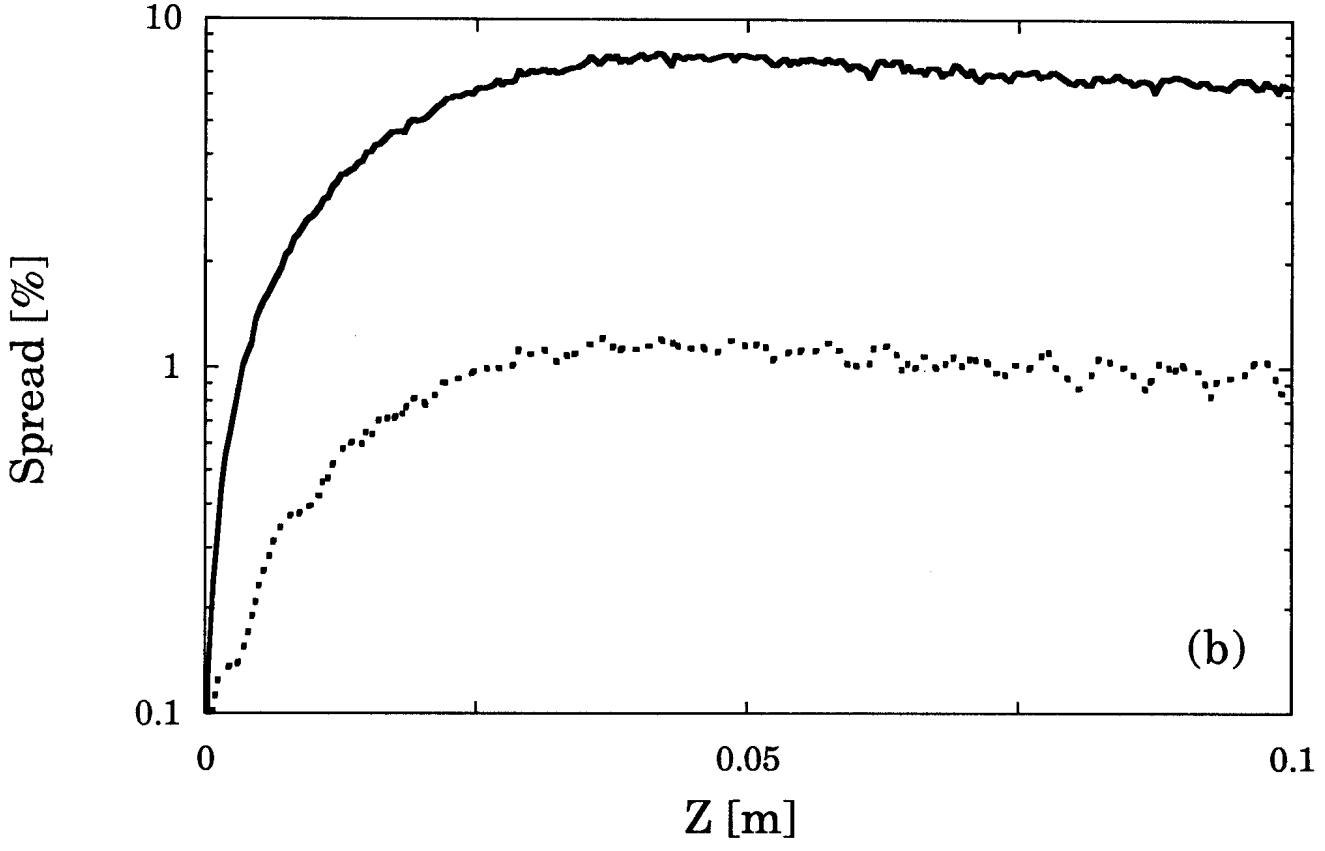

Figure 4

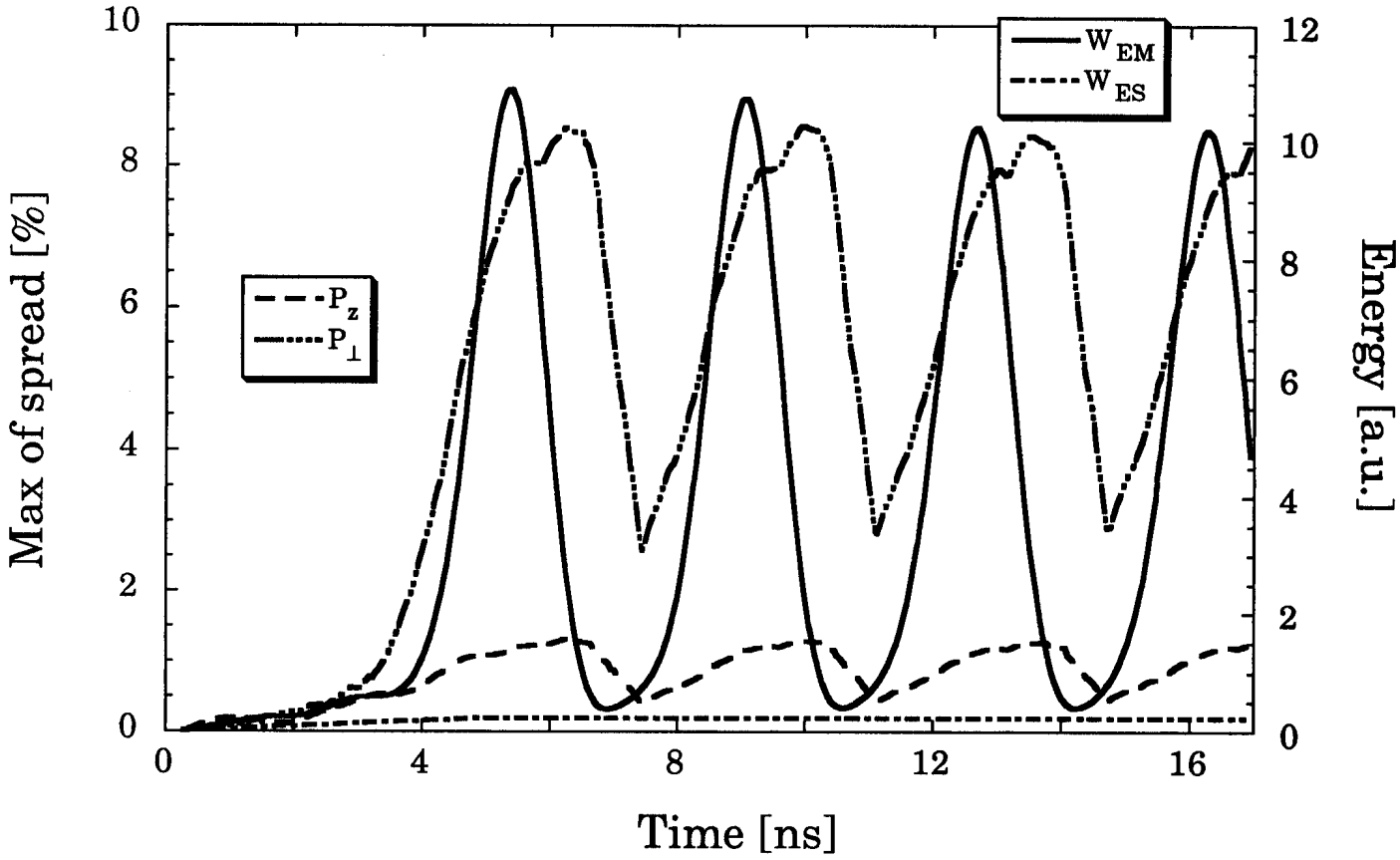

Figure 5

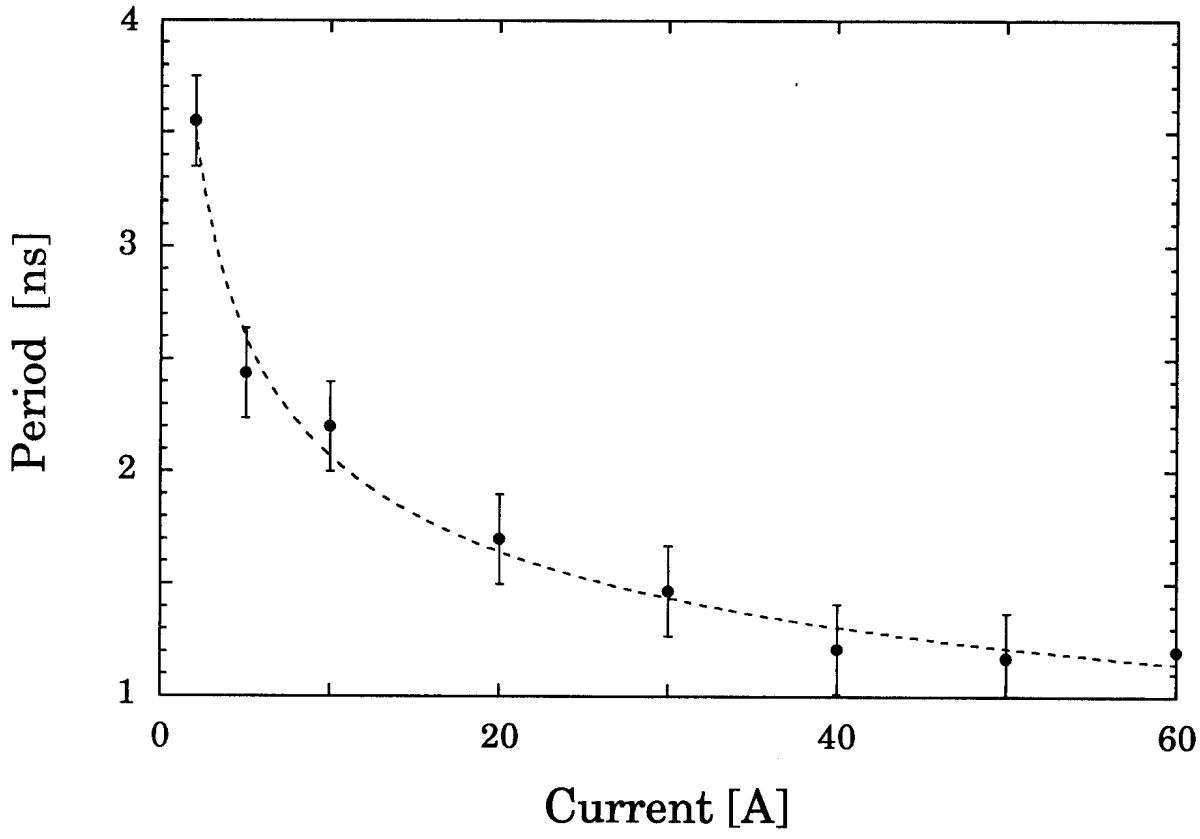

Figure 6

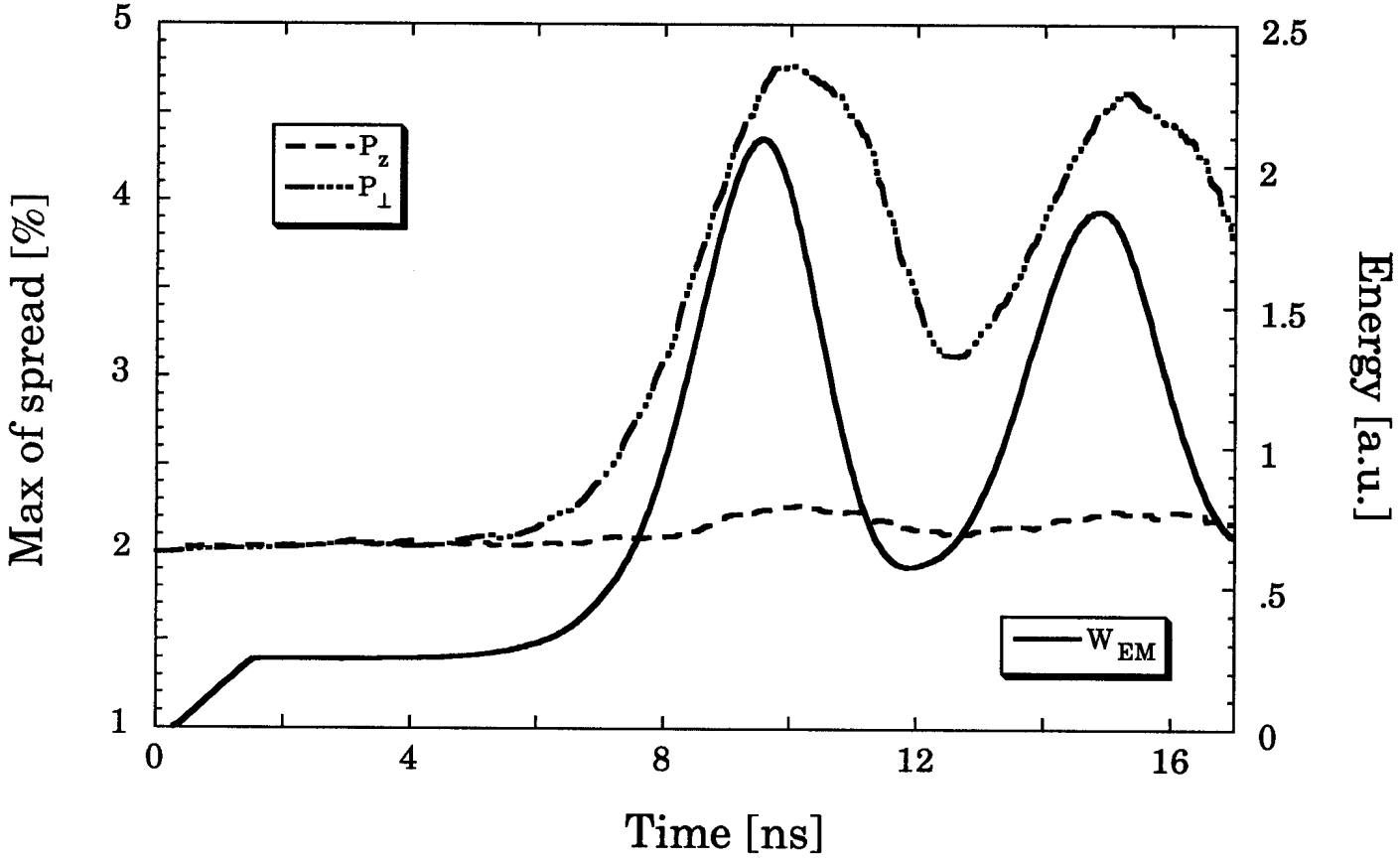
Max of spread [%]
Energy [a.u.]
Time [ns]
P_z
$P_\perp$
W_{EM}
5
4
3
2
1
2.5
2
1.5
1
.5
0
0
4
8
12
16

Figure 7

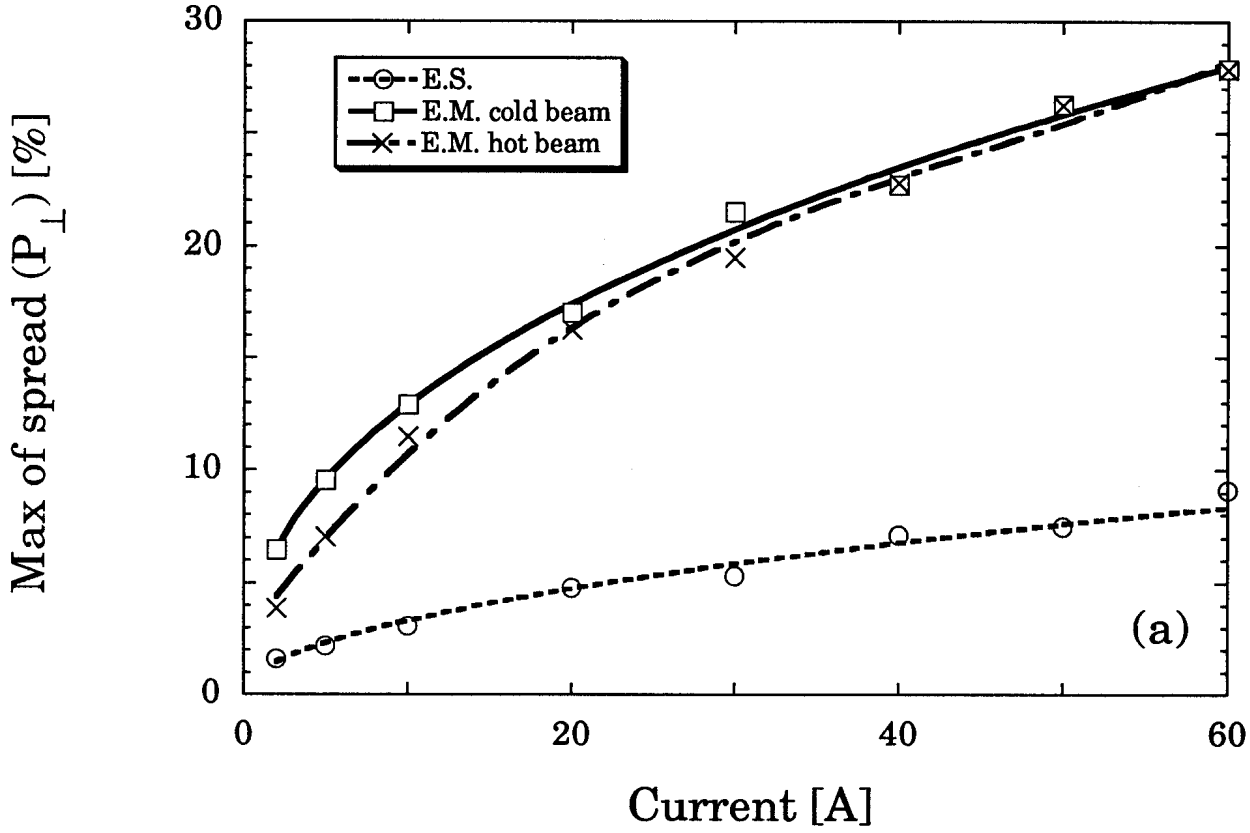

Figure 8

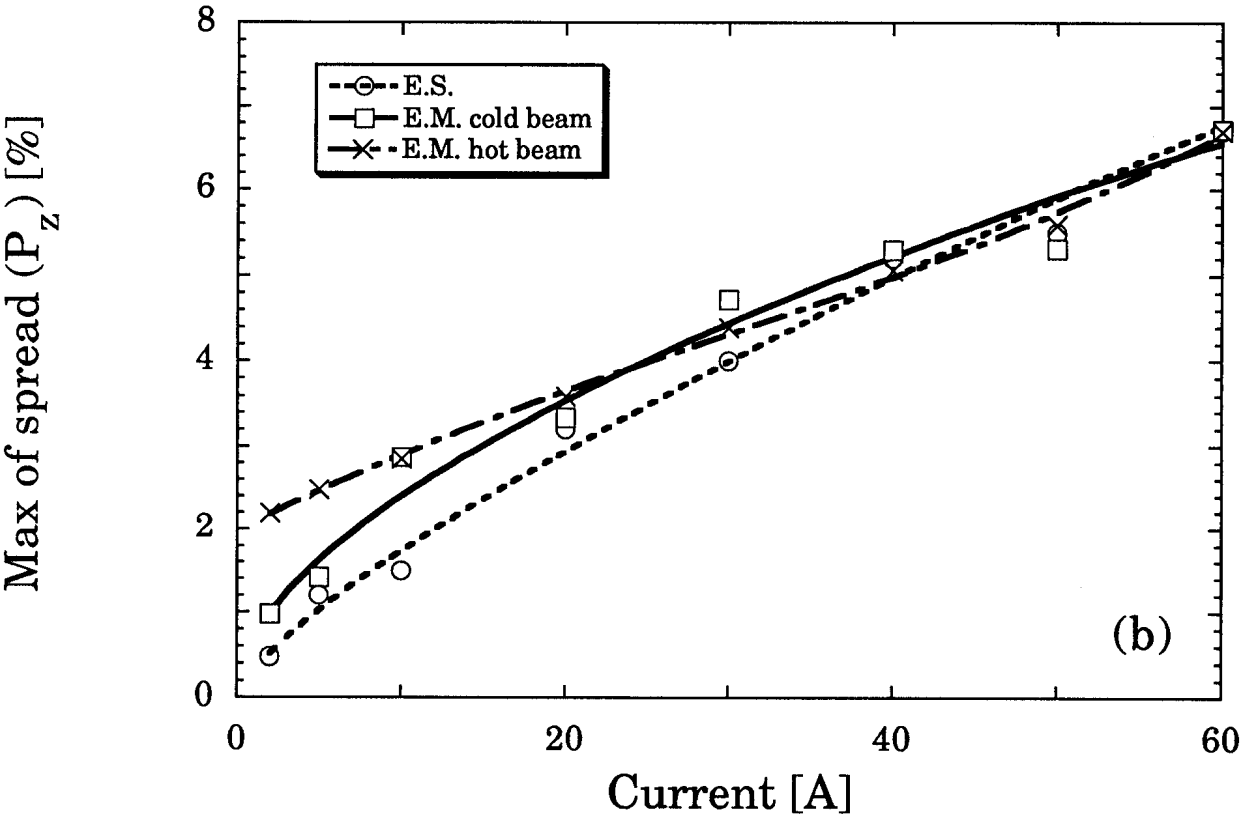

Figure 8